Kinetics of Biaxial Dome Formation by Transformation Superplasticity of Titanium Alloys and Composites

MEGAN FRARY, CHRISTOPHER SCHUH, and DAVID C. DUNAND

By thermally cycling through their transformation temperature range, coarse-grained polymorphic materials can be deformed superplastically, owing to the emergence of transformation mismatch plasticity (or transformation superplasticity) as a deformation mechanism. This mechanism is presently investigated under biaxial stress conditions during thermal cycling of unalloyed titanium, Ti-6Al-4V, and their composites (Ti/10 vol. pct TiC_p, Ti-6Al-4V/10 vol. pct TiC_p, and Ti-6Al-4V/5 vol. pct TiB_w). During gas-pressure dome bulging experiments, the dome height was measured as a function of forming time. Adapting existing models of biaxial doming to the case of transformation superplasticity where the strain-rate sensitivity is unity, we verify the operation of this deformation mechanism in all experimental materials and compare the biaxial results directly to new uniaxial thermal cycling results on the same materials. Finally, existing thickness distribution models are compared with experimentally measured profiles.

I. INTRODUCTION

TITANIUM alloys and titanium matrix composites are useful materials in aerospace applications due to their high strength and stiffness, good corrosion resistance, and low density.[1] Although, at elevated temperature, titanium matrix composites typically exhibit low tensile ductility, they can be made superplastic by repeatedly cycling through their α/β transformation temperature range while applying an external stress.[2] Polymorphic thermal cycling causes internal strains in these materials due to the volume change associated with the transformation, $\Delta V/V$, and the mismatch in the strengths and stiffnesses of each phase. Upon heating through the transformation range, the weaker polymorphic phase undergoes plastic flow (*i.e.*, by creep at high homologous temperatures) to accommodate these transformation mismatch strains. In the absence of applied stress, the strain of transformation is generally reversible upon cooling through the transformation range. However, if a small external biasing stress is applied, deformation occurs preferentially in the direction of the applied stress during each transformation. The strain increment developed after a full thermal cycle (*i.e.*, two transformations) has been found to be proportional to the applied stress,[3] indicating that the deformation is Newtonian (*i.e.*, the stress exponent is unity). This type of deformation is known as transformation-mismatch plasticity, or when large strains are accumulated upon repeated cycling, transformation superplasticity. Greenwood and Johnson[3] developed a continuum-mechanics model of

transformation superplasticity that predicts this linear relationship between the strain increment, $\Delta\varepsilon$, after one thermal cycle and the external biasing stress, σ.

$$\Delta\varepsilon = \frac{4}{3}\frac{\Delta V}{V}\frac{5n}{4n+1}\frac{\sigma}{\sigma_i} \quad [1]$$

where σ_i is the internal stress due to transformation, and n is the creep stress exponent of the weaker phase.

The model of Greenwood and Johnson[3] assumes an isothermal transformation, which is not typically observed in two-phase alloys, such as Ti-6Al-4V. Schuh and Dunand[4] studied the temperature and time dependencies of transformation superplasticity in Ti-6Al-4V by varying the amplitude and frequency of the thermal cycles, and they examined how a partial-phase transformation affects the transformation-superplasticity strain rate. These authors developed a more complex model to describe nonisothermal transformations but established that Greenwood and Johnson's[3] isothermal model (Eq. [1]) can be used as a fair approximation.

Most research on transformation superplasticity has focused on uniaxial deformation of iron and steels,[3,5–10] titanium,[11,12,13] titanium alloys,[3,11,12,14] zirconium,[3,13,15] zirconium alloys,[16,17] cobalt,[3,18] and uranium.[3,19,20] Recently, the linear dependence of Eq. [1] has been also observed under uniaxial conditions in intermetallics (*e.g.*, super α_2 Ti_3Al[21]), metal-matrix composites (*e.g.*, Ti/TiC_p,[22,23] Ti-6Al-4V/TiC_p,[24] and Ti-6Al-4V/TiB_w[25]), and ceramics (Bi_2O_3[26,27]). Deformation under a multiaxial stress state may also be enhanced by transformation superplasticity. For example, more rapid powder densification can be achieved by thermal cycling about the phase transformation during hot pressing, as shown for powders of white cast iron[28] and titanium.[29] Foaming of porous titanium containing pressurized pores can also be enhanced with transformation superplasticity.[30,31] One final example of transformation superplasticity using multiaxial stress is the gas-pressure forming of a thin disk clamped around its periphery, which is also the focus of the present study. Unlike the previous examples, free bulging involves a well-characterized stress state and represents a standard for the study

MEGAN FRARY, previously Graduate Student, Department of Materials Science and Engineering, Northwestern University, is Research Engineer, Caterpillar, Inc., Technical Center, Peoria, IL 61656. CHRISTOPHER SCHUH, previously Graduate Student, Department of Materials Science and Engineering, Northwestern University, is Postdoctoral Fellow, Materials Science and Technology Division, Lawrence Livermore National Laboratory, Livermore, CA 94551. DAVID C. DUNAND, Associate Professor, is with the Department of Materials Science and Engineering, Northwestern University, Evanston, IL 60208.
Manuscript submitted March 23, 2001.

of multiaxial superplasticity, as well as a typical proof-of-concept experiment for superplastic forming of complex shapes into dies.[2]

Biaxial-dome formation occurring by transformation superplasticity has been investigated only once before, by Dunand and Myojin,[32] who observed greater strains after multiple thermal cycles in Ti-6Al-4V and Ti-6Al-4V/TiC$_p$ composites (as compared to isothermal deformation). While it demonstrated that transformation superplasticity enhances deformation, their study did not present kinetic data describing the growth of domes under biaxial stress or model the biaxial problem in the framework of Greenwood and Johnson's uniaxial model. The goal of the present article is to address these issues. Specifically, we investigate the kinetics of dome formation during gas-pressure forming of Ti-6Al-4V and Ti-6Al-4V/TiC$_p$ (the same materials used in Reference 32), as well as commercial-purity titanium (CP-Ti), Ti/TiC$_p$, and Ti-6Al-4V/TiB$_w$. We also adapt an existing model of biaxial doming to include Greenwood and Johnson's constitutive law (Eq. [1]) and compare the predicted deformation kinetics with the experimental results. Finally, the biaxial results are compared with new uniaxial data obtained during thermal cycling of the same materials.

II. EXPERIMENTAL PROCEDURES

A. Experimental Materials

All materials were fabricated by Dynamet Technology (Burlington, MA) using their CHIP process,[33,34] which consists of blending elemental metallic powders, cold isostatic pressing, vacuum sintering, and, finally, containerless hot isostatic pressing. The process was used to fabricate CP-Ti and Ti-6Al-4V, with and without discontinuous reinforcements. Specifically, TiC particles in the amount of 10 vol. pct were added to both CP-Ti and Ti-6Al-4V (these composites will be referred to simply as Ti/TiC$_p$ and Ti-6Al-4V/TiC$_p$ hereafter). Also, Ti-6Al-4V reinforced with 5 vol. pct TiB whiskers (referred to as Ti-6Al-4V/TiB$_w$ hereafter) was synthesized by including TiB$_2$ particulates during blending, which subsequently dissolved and reprecipitated as TiB whiskers during sintering and hot isostatic pressing.[35,36,37]

Because the microstructures of the experimental materials have been extensively examined in the literature (e.g., in References 22 and 32-34), they are only briefly described here. CP-Ti is single phase with large α-grains with an average diameter of about 200 μm, while Ti-6Al-4V exhibits a microstructure common to two-phase $\alpha + \beta$ alloys, with α-phase laths about 80 μm in length separated by β phase, in the amount of about 10 vol. pct at room temperature. Typical TiC particles (in either matrix) are about 20 μm in diameter and are near equiaxed. Finally, the TiB whiskers are known to be randomly oriented (in composites with twice the volume fraction used in this work[25]) with a length greater than 30 μm and a diameter of about 5 μm.

Tensile specimens and disks of each material were machined from near-net-shape densified billets and plates with density greater than 99 pct. The tensile specimens were cylindrical with 20-mm-gage length and 5-mm-gage diameter, while the disks had a diameter of 62 mm and a thickness ranging from 1.36 to 1.59 mm (listed in Table I). Before testing, biaxial disk specimens were coated with Deltaglaze 153, a borosilicate glass paste from Acheson Colloids (Port Huron, MI), which forms a continuous coating upon exposure for 20 minutes at 950 °C, thus preventing contamination with residual atmospheric gases and decreasing surface reflectivity (for more efficient radiative heating).

B. Uniaxial Experiments

Uniaxial tensile experiments were conducted in a custom creep apparatus described in Reference 15, which allowed for rapid thermal cycles under a high-purity argon atmosphere. The temperature was monitored with a K-type thermocouple on the specimen gage and controlled to within ±1 K. Thermal cycles were symmetric triangles through the α/β transformation range of the matrix, with the temperature ranges and frequencies listed in Table I. For each material, thermal-cycling experiments were performed under several uniaxial stresses (ranges of stress for each material are also presented in Table I). The plastic strain of the specimen after each thermal cycle was measured with a linear voltage-displacement transducer at the cold end of the load train, and the reported values are averages over several consecutive thermal cycles.

C. Biaxial Experiments

1. Apparatus

The apparatus for performing biaxial doming experiments is shown in Figure 1 and is described in greater detail in Reference 38. The disk specimens were clamped (using threaded Inconel rods and nuts) into an INCONEL* pressur-

---

*INCONEL is a trademark of INCO Alloys International, Huntington, WV.

---

ization vessel with an open die radius of 24 mm. The specimen and pressurization vessel were placed in a quartz tube under a flowing inert-argon atmosphere at ambient pressure and heated by a radiant area heater with maximum power density of 32 W/cm^2 situated about 6 cm above, and parallel to, the specimen surface. Measurements of the dome height were taken without contacting the specimen, using a laser extensometer (from LaserMike, Dayton, OH) perpendicular to the quartz tube, as described in more detail in the next section.

2. Thermal Cycling Experiments

The specimens were heated to 840 °C in about 2 minutes and held at that temperature for 6 to 8 minutes. The specimen holder was then pressurized to 207 kPa (30 psi) above ambient pressure, and the temperature cycling was initiated. Table I indicates the thermal-cycle frequencies and amplitudes used for each specimen. The cycles used for the biaxial experiments had smaller amplitudes than those used in the uniaxial experiments due to limitations of the radiant heating system used for the former experiments. Longer thermal cycles were performed for the Ti-6Al-4V-based materials due to the slower transformation kinetics.[39] Multiple cycles were performed for approximately 100 minutes, corresponding to 25 cycles for CP-Ti and Ti/TiC$_p$ and about 12 cycles for Ti-6Al-4V-based materials. The dome was then cooled for about 20 minutes, and its height was measured (with an accuracy of about 0.1 mm) with the laser extensometer at a temperature of about 150 °C. This procedure was repeated several times for each specimen, giving a history of the

Table I. Experimental Materials and Conditions

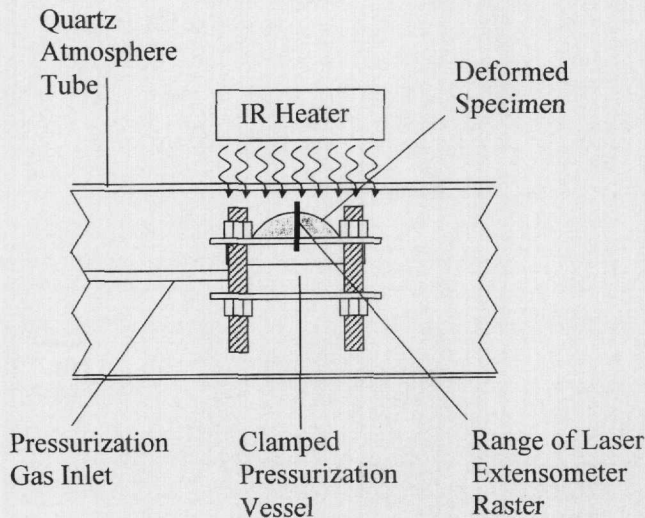|		Uniaxial			Biaxial			
Material	Cycle Frequency (h^{-1})	Cycle Temperature (°C)	Stress Range (MPa)	Cycle Temperature (°C)	Gas Pressure (MPa)	Original Sheet Thickness* (mm)	Final Apex Thickness (mm)	Von-Mises Apex Strain
CP-Ti	15	840 to 970	0.4 to 7.0	840 to 965	0.20	1.390	0.636	0.78
Ti/10 TiC$_p$	15	840 to 1000	0.4 to 7.0	840 to 970	0.20	1.360	0.759	0.58
Ti-6Al-4V	7.5	840 to 1030	0.6 to 6.0	840 to 970	0.20	1.391	0.878	0.46
Ti-6Al-4V/10 TiC$_p$	7.5	840 to 1030	1.5 to 6.5	840 to 970	0.20	1.510	1.179	0.25
Ti-6Al-4V/5 TiB$_w$	7.5	840 to 1030	0.5 to 5.0	840 to 980	0.20	1.590	1.372	0.15

*Maximum variation of 38 μm.

Fig. 1—Schematic of the experimental biaxial gas-pressure apparatus, showing the central section of the quartz atmosphere tube, with a deformed specimen clamped in the pressurization vessel. The range of laser extensometer raster is also shown.

dome height. After 3 to 5 sets of cycles, the specimen holder was removed from the quartz tube, and a measurement of the dome height was taken with calipers to verify the laser measurements. Negligible discrepancies (at most 0.3 mm) were found. Experiments were terminated after times ranging from 15,840 seconds (for CP-Ti) to 54,720 seconds (for Ti-6Al-4V) with no dome rupture.

3. Thickness Profile Determination

Each dome was sectioned along a diameter with a high-speed diamond blade, and digital images were taken of the resulting cross section. The thickness distribution was found as a function of position along the dome by image analysis. An edge-finding algorithm was used to locate the upper and lower surface of the dome from which average thickness values were determined at equiangular steps of 0.02 radians along the dome profile. Thickness measurements equally distant from the dome apex and on opposite sides of the profile were averaged. Mirror symmetry was observed to within 60 μm, indicating uniform deformation (unlike earlier experiments in Reference 32, where the specimens were oriented vertically and slumped under the action of gravity). On several specimens, a point micrometer was used to measure the thickness at various points on the dome surface.

Within experimental accuracy, this procedure yielded identical measurements to those obtained through the image analysis procedure, validating the accuracy of this method.

III. RESULTS

A. Uniaxial Deformation

In Figure 2, the uniaxial strain increment measured upon each thermal cycle is plotted as a function of the applied uniaxial tensile stress. The relationship is linear at low applied stresses for all of the experimental materials, as expected from Eq. [1]. The slope in the linear regime, $d\Delta\varepsilon/d\sigma$, is also given for each material in Table II. At higher applied stresses, some deviation from linearity is observed for CP-Ti and Ti/TiC$_p$, as power-law creep emerges as the dominant deformation mechanism. This transition has been observed in many materials exhibiting transformation superplasticity.[3,4,15,21,40]

B. Biaxial Deformation

The dome height, as measured by laser extensometer, is shown as a function of time in Figure 3. The curves display the typical shapes of isothermal, constant-pressure biaxial-doming experiments where fine-grain superplasticity is the active deformation mechanism:[41-46] the deformation, which is initially very rapid, becomes slower as the dome height increases. As expected, the weakest material, CP-Ti, deformed most rapidly, while the Ti-6Al-4V-based materials deformed more slowly due to the longer thermal cycle times and higher creep resistance. Photographs of the CP-Ti and Ti/TiC$_p$ domes are shown in Figure 4. The thickness profiles for each specimen are displayed in Figure 5, in terms of relative thickness, s/s_0, where s is the current thickness, and s_0 is the initial thickness (given in Table I). The error bars correspond to the standard deviation over the averaging range of 0.02 radians. As expected, dome height (Figure 3) is correlated with apex-thickness reduction (Figure 5): CP-Ti bulged most and is thinnest at the apex, while Ti-6Al-4V/TiB$_w$ is the least bulged and thickest at the apex. Final apex-thickness values are listed in Table I, together with von Mises equivalent strains (assuming equibiaxial strains at the apex). The most deformed CP-Ti sheet exhibits a true apex strain of 0.78, corresponding to an engineering strain of 119 pct.
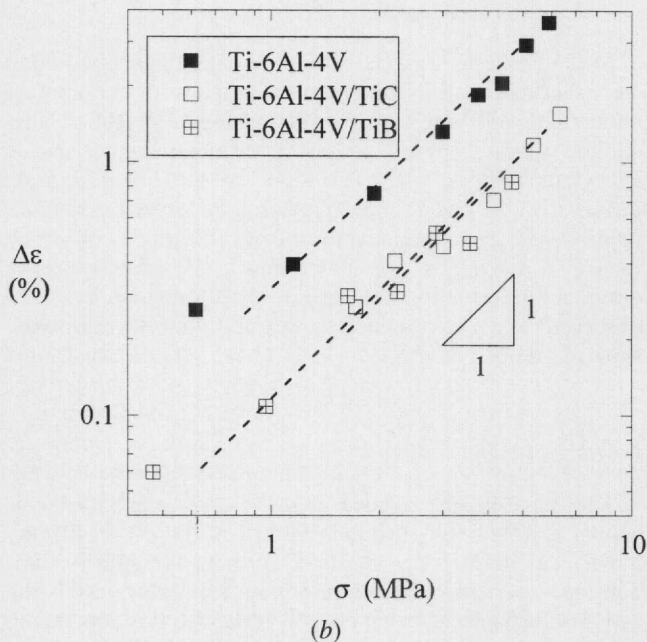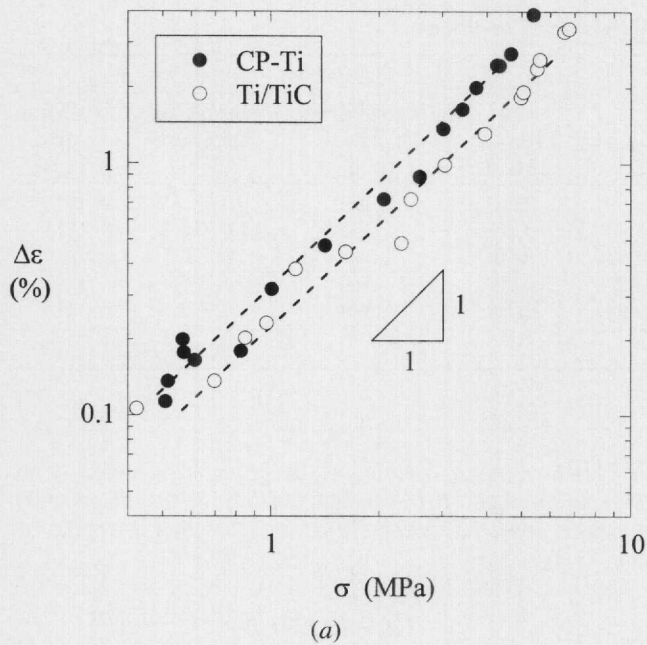
(a)

σ (MPa)

Fig. 3—Dome height as a function of time for each material.

(b)

σ (MPa)

Fig. 2—Tensile strain increment Δε after each thermal cycle under uniaxial stress σ, for (a) CP-Ti and its composite and (b) Ti-6Al-4V and its composites.

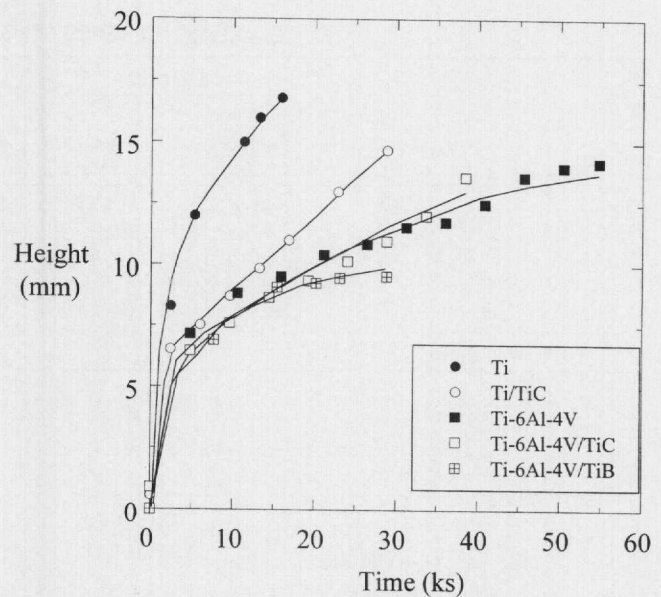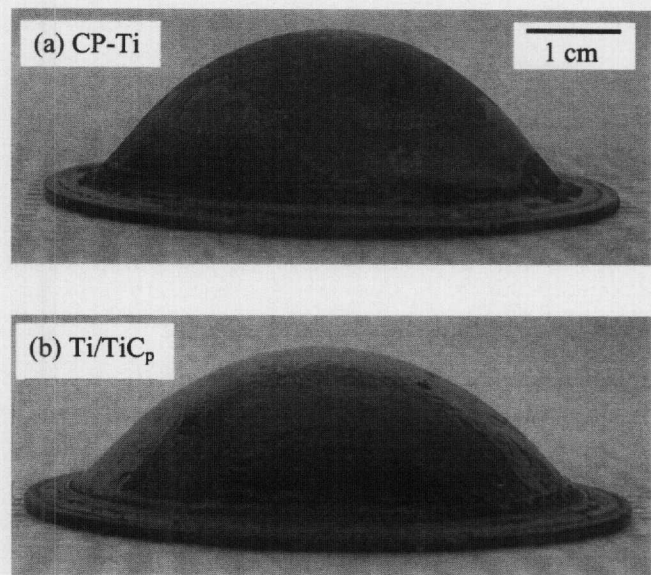Fig. 4—Photographs of (a) CP-Ti and (b) Ti/TiC$_p$ domes.

Table II. Comparison of Fitted Biaxial, Experimental Uniaxial, and Literature Values for the Transformation Superplasticity Constants K_{TSP} and $d\Delta\varepsilon/d\sigma$

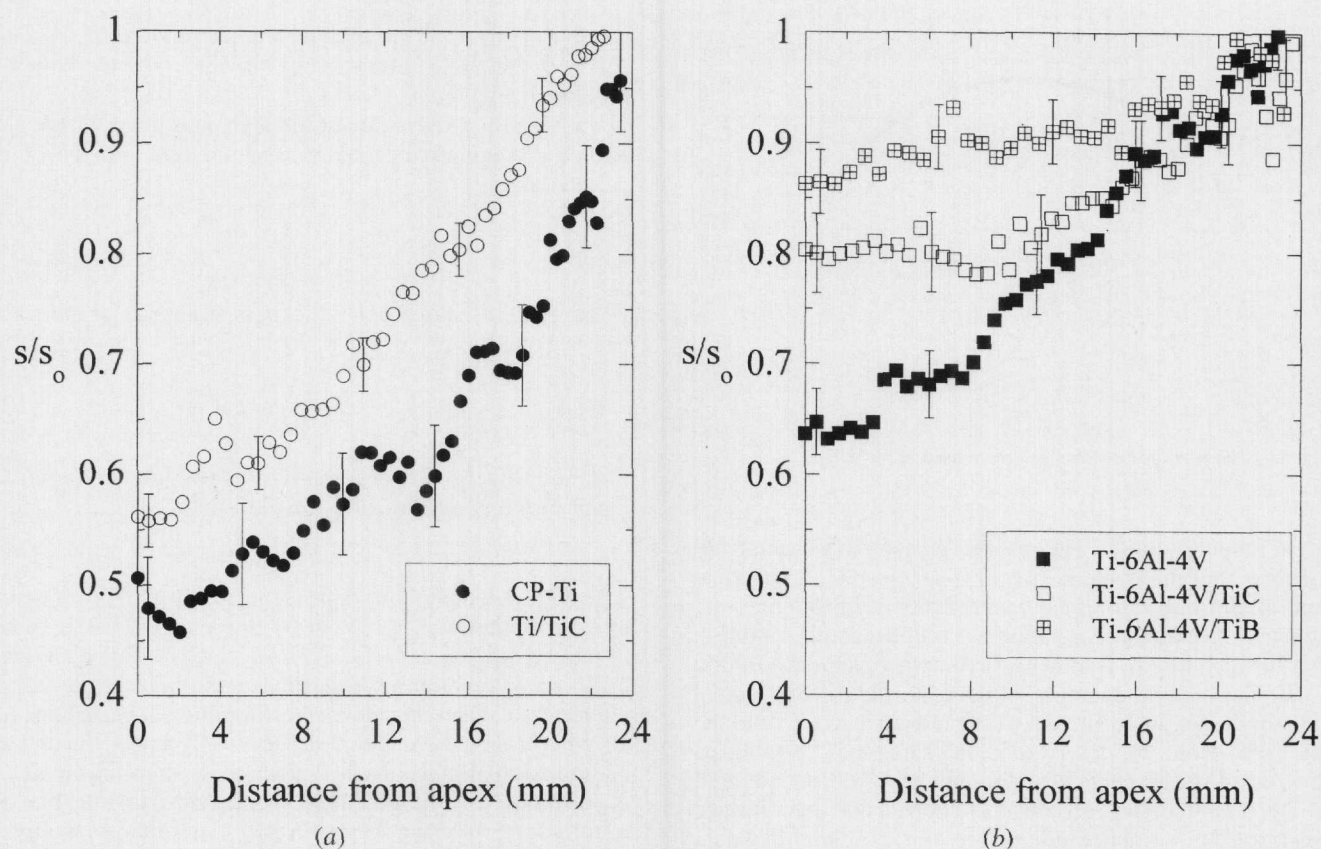|	Experimental			Literature Values		
	K_{TSP} Biaxial* $(10^{12}$ Pa$^{-1} \cdot$ s$^{-1})$	K_{TSP} Uniaxial $(10^{12}$ Pa$^{-1} \cdot$ s$^{-1})$	$d\Delta\varepsilon/d\sigma$ (GPa^{-1})	K_{TSP} Uniaxial $(10^{12}$ Pa$^{-1} \cdot$ s$^{-1})$	$d\Delta\varepsilon/d\sigma$ (GPa^{-1})	Reference
CP-Ti	—	12	2.9	2.6 to 14.1	2.3 to 3.4	11, 23, 24
Ti/10 TiC$_p$	4.2	9.2	2.2	5.0 to 13.3	2.4 to 12.5	22, 23, 24
Ti-6Al-4V	—	8.3	4.0	4.4 to 6.7	2.1 to 3.2	4, 11, 25
Ti-6Al-4V/10 TiC$_p$	2.5	3.5	1.7	2.3	1.1	24, 40
Ti-6Al-4V/5 TiB$_w$	2.4	2.9	1.4	—	—	—

*Best-fit value.

Fig. 5—Thickness profile (normalized by original sheet thickness, s_0) for (*a*) CP-Ti and its composite, and (*b*) Ti-6Al-4V and its composites.

IV. DISCUSSION

A. *Uniaxial Transformation Superplasticity*

The superplastic slope, $d\Delta\varepsilon/d\sigma$, measured for each material at low applied stresses is given in Table II, where existing values from the literature are also presented. In all cases, the new values are in reasonable agreement with previous studies, considering the variability in the thermal-cycle amplitude and frequency between investigations.

The addition of particulate or whisker reinforcements reduces the cycling strain rate, in agreement with previous work on these and similar materials.[24,25,40] However, in the case of Ti/TiC$_p$, previous investigations have demonstrated enhanced superplastic strain increments as compared to unreinforced CP-Ti when large-amplitude cycles with long cycle durations are employed.[22,23] In those studies, the enhanced deformation (about a factor of 2) was attributed to increased mismatch due to the presence of inert, nontransforming particulates and modeled by considering creep relaxation of the additional mismatch. In the present case, the thermal cycles were much shorter (by about 50 pct) and used a smaller thermal amplitude (about 12 pct smaller) than those investigations. Furthermore, the β transus of the CP-Ti used in this work was estimated at 955 °C (73 °C higher than for pure Ti, most probably due to oxygen contamination of powders), based on measurements of the transformation strain signal during thermal cycling. The addition of a small amount of carbon to pure Ti (dissolved from the TiC particulates) is expected to have two effects. First, carbon in solid solution

increases the β-transus temperature by about 40 K in titanium.[47] Second, the α/β transformation requires redistribution of carbon, since the α phase has about twice the carbon solubility of the β phase.[47] Therefore, the transformation in Ti/TiC$_p$ is expected to occur at very high temperatures (about 995 °C) and to be kinetically limited by the diffusion of carbon through the matrix. Then, the combination of rapid thermal cycles and small superheating above the β transus (about 5 °C) is likely to lead to incomplete phase transformations during cycling. As discussed in References 4 and 15, incomplete transformations significantly decrease the measured strain increments during thermal cycling and can easily account for the differences between the measured values of $d\Delta\varepsilon/d\sigma$, and those reported in the literature.[22,23,24]

B. *Modeling Biaxial Deformation*

The following discussion of biaxial doming uses the same assumptions used in the first detailed description of biaxial deformation by Jovane,[41] *i.e.*, isotropy, incompressibility, negligible bending effects, power-law deformation, and a spherical geometry. However, we account for the variation in stress along the dome profile and for the nonuniform thickness distribution, as done by later authors.[44,45,48] In addition, we consider the operation of two deformation mechanisms (power-law creep and transformation superplasticity). Based on the developments of Enikeev and Kruglov,[45] we also directly derive a compact differential equation for the rate of change in the dome height, which can be numerically solved to determine the full height history
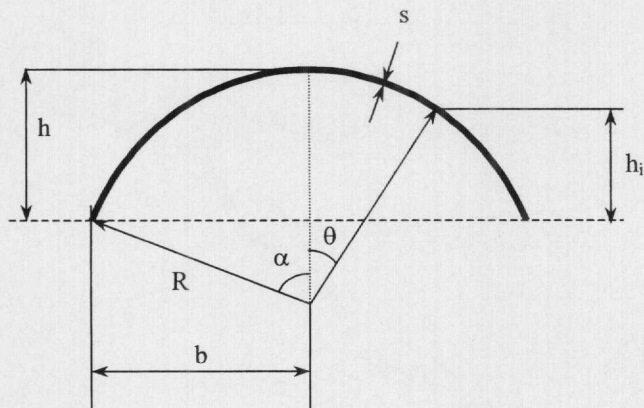
Fig. 6—Schematic of the dome geometry used in modeling.

of a bulging dome. The model presented subsequently assumes that the dome is part of a sphere (*i.e.*, a spherical cap) at all times during the experiments. By examining the dome profiles after deformation, we found that this condition was fulfilled for all specimens, as described in the Appendix.

For the doming geometry (Figure 6), the three principal stresses are the hoop stress, σ_h, the radial stress, σ_r, and the thickness stress, σ_s, described in an orthogonal, curvilinear-coordinate system centered at the apex of the dome and fitted to the dome surface. Because of the traction-free surface condition on the upper side of the thin disk, the thickness stress is small enough that it may be neglected. The radial stress at any point within the dome with thickness, s, can be determined by thin shell theory as[41]

$$\sigma_r = \frac{p \cdot R}{2 \cdot s} \qquad [2]$$

where p is the gas pressure, and R is the radius of curvature of the dome. Due to the geometric constraint at the dome edge, a plane-strain state exists in this region, with the hoop stress given as[44]

$$\sigma_h = \frac{\sigma_r}{2} \qquad [3]$$

and the radial (ε_r), thickness (ε_s), and hoop (ε_h) strains as[49]

$$\varepsilon_r = -\varepsilon_s \qquad [4a]$$

$$\varepsilon_h = 0 \qquad [4b]$$

However, at the apex, the stress state is balanced biaxial:[41]

$$\sigma_h = \sigma_r \qquad [5]$$

$$\varepsilon_r = \varepsilon_h = -2 \, (\varepsilon_s) \qquad [6]$$

The von Mises equivalent stress, σ_{eq}, and strain rate, $\dot{\varepsilon}_{eq}$, at the apex may thus be found as

$$\sigma_{eq} = \sigma_r \qquad [7a]$$

$$\dot{\varepsilon}_{eq} = -\dot{\varepsilon}_s \qquad [7b]$$

Based on the deformation of a half-meridian, the thickness at the apex, s_a, has been derived by Enikeev and Kruglov[45] as

$$s_a = s_0 \cdot \left(\frac{\sin \alpha}{\alpha}\right)^2 \qquad [8]$$

where s_0 is the uniform thickness of the undeformed sheet, and α is the angle subtended by the apex and the edge of the dome (Figure 6).

The effective strain rate at the apex was given in Eq. [7] as being equal to the thickness strain rate, $\dot{\varepsilon}_s$, which is defined as

$$\dot{\varepsilon}_s = \frac{\dot{s}_a}{s_a} \qquad [9]$$

Using Eqs. [8] and [9], the thickness strain rate at the apex can be found as

$$\dot{\varepsilon}_s = -2\dot{\alpha} \cdot \left(\frac{1}{\alpha} - \cot \alpha\right) \qquad [10]$$

A simplified uniaxial constitutive law that can describe many different deformation mechanisms is

$$\dot{\varepsilon} = K \cdot \sigma^n \qquad [11]$$

where K is a temperature-dependent parameter. For transformation superplasticity, the stress exponent, n, has a value of unity at low stresses (Eq. [1]). However, during a thermal cycle, transformation superplasticity contributes to the deformation only when the phase transformation is occurring. At all other times, the material deforms only under the action of the external stress by a typical creep mechanism (*e.g.*, dislocation creep). Since these two mechanisms operate at different times during the cycle, they contribute to the total deformation independently, and it is reasonable to add their contributions:[50]

$$\dot{\varepsilon} = \dot{\varepsilon}_{creep} + \dot{\varepsilon}_{TSP} = K_{creep} \cdot \sigma^n + K_{TSP} \cdot \sigma \qquad [12]$$

Equation [12] is a simple constitutive creep law valid only for the uniaxial case. To find the thickness strain rate, a more generalized equation involving the multiaxial stress state is required:[51]

$$\dot{\varepsilon}_1 = K_{creep} \cdot \sigma_{eq}^{n-1} \cdot \left[\sigma_1 - \frac{1}{2}(\sigma_2 + \sigma_3)\right]$$
$$+ K_{TSP} \cdot \left[\sigma_1 - \frac{1}{2}(\sigma_2 + \sigma_3)\right] \qquad [13]$$

where 1, 2, and 3 are the principle directions. Upon introduction of Eqs. [2] and [7] into Eq. [13], the thickness strain rate at the apex is found as

$$\dot{\varepsilon}_s = - K_{creep} \cdot \sigma_r^n - K_{TSP} \cdot \sigma_r \qquad [14]$$

Combining Eqs. [2], [10], and [14] then results in

$$K_{creep} \cdot \left(\frac{pR}{2s_a}\right)^n + K_{TSP} \cdot \frac{pR}{2s_a} = 2\dot{\alpha} \cdot \left(\frac{1}{\alpha} - \cot \alpha\right) \qquad [15]$$

The preceding equation is equivalent to Eq. [7] in Reference 45, for the case of a single deformation mechanism (*i.e.*, $K_{TSP} = 0$). Substituting Eq. [8] and noting that $R = b/\sin \alpha$ (Figure 6), Eq. [15] becomes

$$K_{creep} \cdot \left(\frac{pb}{2s_0} \frac{\alpha^2}{\sin^3 \alpha}\right)^n + K_{TSP} \cdot \frac{pb}{2s_0} \frac{\alpha^2}{\sin^3 \alpha} = 2\dot{\alpha}$$
$$\cdot \left(\frac{1}{\alpha} - \cot \alpha\right) \qquad [16]$$

Defining the nondimensional apex height, $\eta = h/b$, which is equal to zero when the disk is flat and unity at a hemisphere, and noting that $\eta = \tan(\alpha/2)$ from geometry, Eq. [16] can be rewritten as

$$\dot{\eta} = \frac{1}{2} \cdot \frac{\eta \cdot \arctan \eta \cdot (1 + \eta^2)}{\eta - \arctan \eta \cdot (1 - \eta^2)} \cdot [K_{creep} \cdot S^n + K_{TSP} \cdot S]$$

[17]

where

$$S = \frac{pb}{4s_0} \cdot \frac{\arctan^2 \eta \cdot (1 + \eta^2)^3}{\eta^3}$$

[18]

Equation [17] thus presents a simple differential equation for the rate of change in the dome height, as a function of the temperature, forming pressure, instantaneous height, initial sheet thickness and radius, and known materials parameters. In the sections to follow, we numerically evaluate Eq. [17] to predict the apex height history during thermal-cycling experiments, first, for the unreinforced materials and, later, for the metal-matrix composites.

C. Biaxial Deformation of CP-Ti and Ti-6Al-4V

We first discuss the model predictions for CP-Ti and Ti-6Al-4V, as the values of the prestress deformation constants, K_{TSP} and K_{creep}, are well characterized by uniaxial experiments, and the model can thus be implemented without the use of any adjustable parameters.

In the case of CP-Ti, we consider the contributions from both creep and transformation superplasticity. For the latter mechanism, the superplastic slope, $d\Delta\varepsilon/d\sigma = 2.3$ GPa^{-1}, has been determined from several studies[11,23,24] with different cycle amplitudes and frequencies, after accounting for extraneous creep contributions to the total deformation. Furthermore, the materials from those studies[11,23,24] were similar to CP-Ti used in the present study, and the total strain increment (which includes both creep and transformation superplastic deformation) found in this work ($d\Delta\varepsilon_{tot}/d\sigma = 2.9$ GPa^{-1}) is close to the values from those studies ($d\Delta\varepsilon_{tot}/d\sigma = 2.3$ to 3.4 GPa^{-1}) before correcting for creep deformation. The prestress constant $K_{TSP} = v \cdot d\Delta\varepsilon/d\sigma$ is then found as 9.58×10^{-12} Pa$^{-1} \cdot$ s^{-1}, using the cycle frequency, v, in Table I. The contribution of creep during a thermal cycle is found by integrating the dislocation creep rate over the portions of the thermal cycle above the β transus (found at 955 °C) and neglecting creep in the more creep-resistant α phase, as discussed in References 22 and 23. The creep law of β-Ti in Reference 52, with a power-law stress exponent of $n = 4.3$, was used. By numerically averaging over the experimentally measured thermal cycles, the effective, average value of K_{creep} during the biaxial-doming experiments is found as 5×10^{-34} Pa$^{-4.3} \cdot$ s^{-1}.

The model predictions for biaxial doming of CP-Ti are compared with the experimental results in Figure 7, and the agreement is very good, especially considering that no adjustable parameters were used. The individual contributions of transformation superplasticity and dislocation creep of β-Ti, found by setting K_{creep} and K_{TSP}, respectively, to zero in Eq. [17] are also shown. Clearly, the biaxial deformation is primarily due to transformation superplasticity with a small but nonnegligible contribution from creep. It should also be
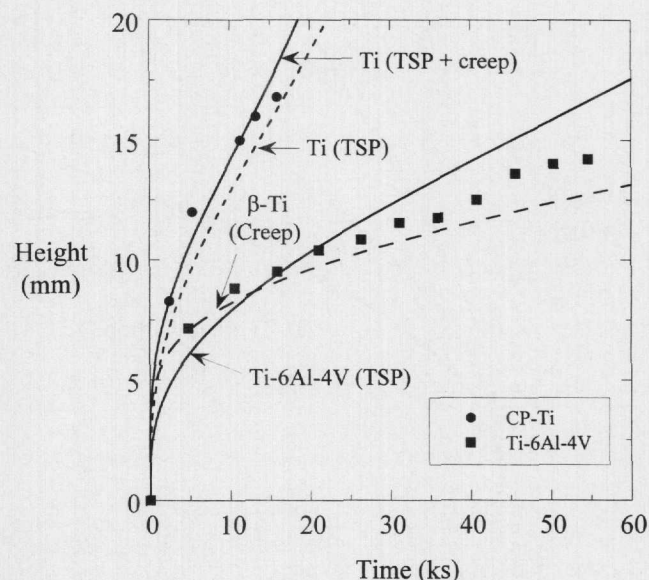

Fig. 7—Experimental time dependence of dome heights for CP-Ti and Ti-6Al-4V. Model predictions (Eq. [17]) are shown for all active deformation mechanisms.

noted that the individual contributions to dome height shown in Figure 7 are not additive; rather, the rates of dome growth are additive according to Eq. [17].

For the case of Ti-6Al-4V, the experimental thermal cycles did not cross the β transus at 1000 °C,[39] so the material is in the process of transforming at all times during the cycle.[4] Thus, all of the measured deformation can be attributed to transformation superplasticity, and no contribution from creep need be added to the model ($K_{creep} = 0$). For 8-minute cycles between 840 °C and 970 °C, Reference 4 gives the superplastic slope, $d\Delta\varepsilon/d\sigma = 1.25$ GPa^{-1}, from which K_{TSP} is found as $v \cdot d\Delta\varepsilon/d\sigma = 2.6 \times 10^{-12}$ Pa$^{-1} \cdot$ s^{-1}. We note that the uniaxial slope found in this study ($d\Delta\varepsilon_{tot}/d\sigma \approx 4$ GPa^{-1}) for a larger temperature amplitude (840 °C to 1030 °C) is larger than the value used here for cycles over the range 840 °C to 970 °C, due to the occurrence of creep above the β transus at 1000 °C. The predictions of the model are compared to the experimental results in Figure 7 and, as for CP-Ti, the agreement is good.

D. Biaxial Deformation of Composite Materials

In contrast to the unreinforced materials, creep and transformation superplasticity characteristics of the composite materials are less thoroughly characterized in uniaxial tension, and the existing studies use different thermal-cycle profiles and/or different volume fractions of reinforcement. Therefore, in this section, we consider K_{TSP} as an adjustable parameter, fit solutions of Eq. [17] to the experimental data, and compare the fitted values of K_{TSP} to those reported previously in the literature, as well as those obtained in the present uniaxial experiments. As already discussed for unreinforced Ti-6Al-4V, transformation superplasticity is the only operative deformation mechanism for the Ti-6Al-4V composites, and there is no contribution from creep. Also, as described previously for Ti/TiC$_p$, the presence of dissolved carbon and oxygen in the CP-Ti matrix increases the β-transus temperature (to about 995 °C), eliminating any
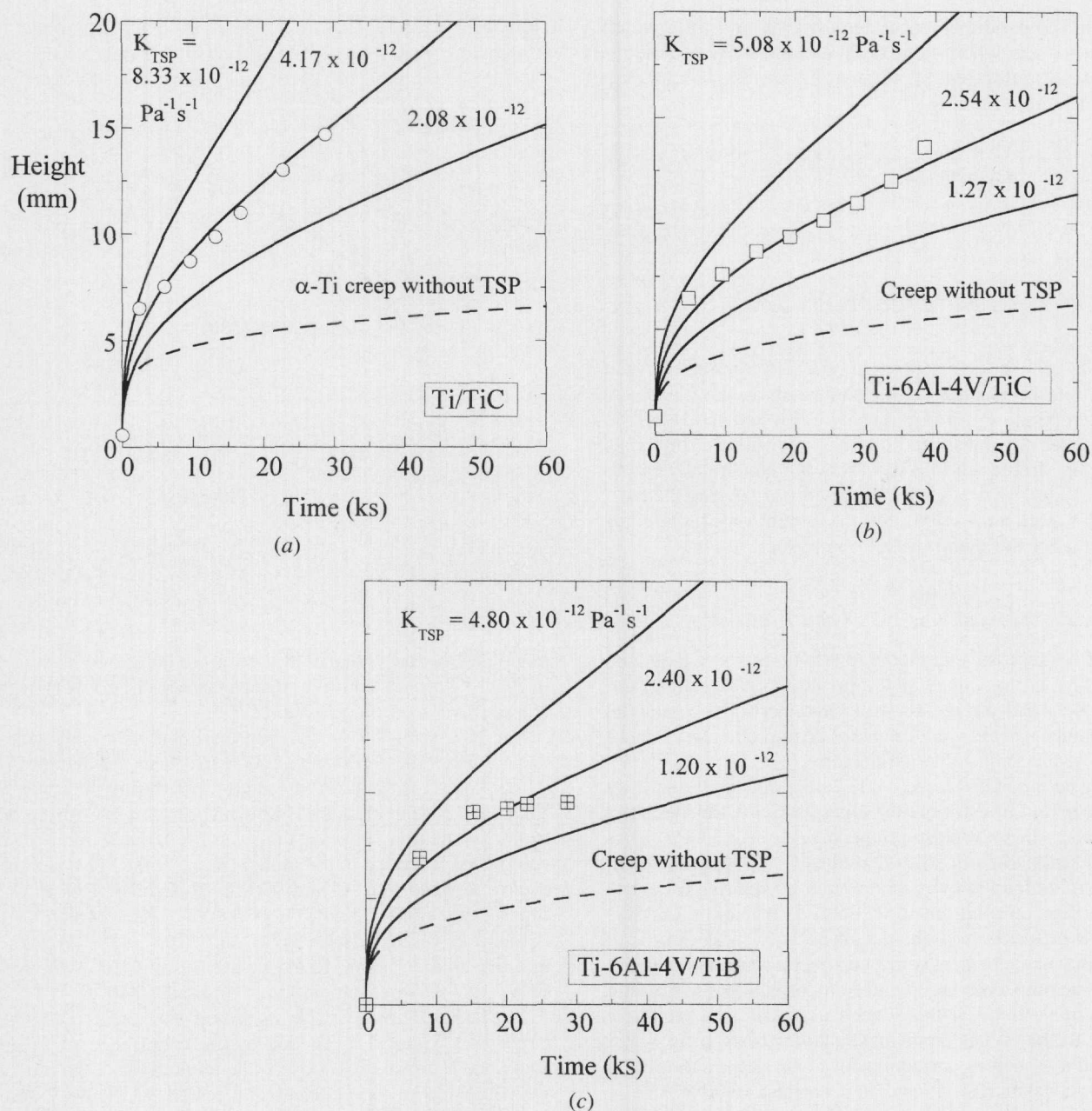
Fig. 8—Comparison of experimental results and model predictions (full line) with different values of K_{TSP} as a fitting parameter for (a) Ti/TiC$_p$, (b) Ti-6Al-4V/TiC$_p$, and (c) Ti-6Al-4V/TiB$_w$. Also shown is the expected amount of creep deformation during thermal cycling (full lines), in the absence of any transformation superplasticity contribution (dashed lines).

excursion into the β field during the biaxial experiments, for which the maximum cycle temperature was 970 °C. Thus, for all of the composite materials, the contribution of creep outside the transformation-temperature range is assumed to be negligible ($K_{creep} = 0$).

In Figures 8(a) through (c), we show the experimental data and model predictions for Ti/TiC$_p$, Ti-6Al-4V/TiC$_p$, and Ti-6Al-4V/TiB$_w$, respectively, using three different values of K_{TSP} for each material. The value of K_{TSP} that best describes the experimental results is listed in Table II, along with the values determined from the uniaxial experiments (Figure 2) and from several previous uniaxial studies on similar materials. For both Ti-6Al-4V composites, the agreement between the fitted values of K_{TSP} and the values from the

present uniaxial experiments is satisfactory (within a factor of 1.4). For both materials, the disagreement is most likely due to the lower cycle amplitudes used for the biaxial experiments (Table I), which eliminate the creep contribution to deformation and limit the extent of the phase transformation. For the case of Ti-6Al-4V/TiB$_w$, whisker alignment during deformation may also reduce the observed value of K_{TSP} due to strain hardening.[25]

A larger disagreement between the uniaxial and biaxial experiments was observed for Ti/TiC$_p$ (Table II). The slower-than-expected bulging is perhaps caused by an incomplete transformation, as discussed previously and in References 23 and 24. In other uniaxial studies,[22–24,53] wide variation in K_{TSP} values has been reported for Ti/TiC$_p$ (Table II),

such that the observed variation by a factor of 2.2 is still reasonable. Again, the cycle amplitude for the biaxial experiments was somewhat lower than for the uniaxial experiments.

The preceding results show that transformation superplasticity can fully account for the measured deformations in all three composites. In what follows, we compare the measured values to upper-bound predictions for deformation by creep alone, in the absence of an enhancement due to the phase transformation. For this purpose, the creep rate of the matrix material (CP-Ti or Ti-6Al-4V) is taken as an upper bound of the creep rate of the respective composite materials, since isothermal creep of the composites is slower than for the unreinforced matrices.[22,24,54,55] For the case of Ti-6Al-4V, the average creep rate during cycling (in the absence of transformation superplasticity) is found by averaging experimental isothermal-creep data[56] over the temperature range of the thermal cycle (840 °C to 970 °C). As discussed previously, it is likely that the matrix of the Ti/TiC$_p$ composite did not fully transform during the present thermal cycles; thus, the creep of α-Ti[52] is considered for comparison with the Ti/TiC$_p$ composites. As before, the expected creep rate during cycling (without transformation) is found by numerical averaging of this creep rate over the thermal cycle.

The amount of dome growth expected by creep during thermal cycling, if there were no enhancement due to the phase transformation, is shown as a dashed line in Figures 8(a) through (c). When compared with these trendlines, the experimental data clearly verify that transformation superplasticity is active during thermal cycling, as creep alone could not result in such large deformation for any of these composites. Although we did not achieve superplastic strains in all of the materials (i.e., engineering thickness strain of 120 pct for CP-Ti and less than 80 pct for all other materials), the operation of the transformation-superplasticity deformation mechanism is further confirmed by this analysis. Thus, if longer experimental times or larger forming pressure were used, superplastic strains (>100 pct) could be achieved, as shown in Reference 32, for Ti-6Al-4V and Ti-6Al-4V/TiC$_p$ domes.

E. Thickness Modeling

In this section, two existing models are presented for predicting the final thickness distribution in the domes. The first was developed by Enikeev and Kruglov,[45] who make the assumption that each meridian passing through the dome apex is uniformly deformed at any point in time. The model also assumes an appropriate variation in stress state from balanced biaxial at the apex to plane strain at the periphery. The authors develop the following equation for the variation in the thickness, s, as a function of position in the dome:

$$s = s_0 \cdot \left(\frac{\sin \alpha}{\alpha}\right)^2 \cdot \frac{\theta}{\sin \theta} \quad [19]$$

where the angle, θ, is illustrated in Figure 6. At $\theta = 0$, this expression reduces to Eq. [8], giving the thickness, s_a, at the dome apex, while at $\theta = \alpha$ at the dome periphery, the thickness is reduced by a factor of $\alpha/\sin \alpha$ (i.e., $s/s_0 = \sin \alpha/\alpha$).

The second thickness-distribution model is that of Ragab,[42] which like that of Enikeev and Kruglov,[45] is based solely on geometry. However, it assumes a balanced, biaxial stress state throughout the dome. The thickness at any point is given as

$$s = s_0 \cdot \left(1 + \frac{h_i \cdot h}{b^2}\right)^{-2} \quad [20]$$

where h_i is the local height of the dome at any radial position. By substituting for h_i, h, and b in terms of α and θ (Figure 6), Eq. [20] becomes

$$s = s_0 \cdot \left(\frac{\cos \alpha + 1}{\cos \theta + 1}\right)^2 \quad [21]$$

At the periphery of the dome ($\theta = \alpha$), Ragab's model[42] (Eq. [21]) predicts no reduction in thickness ($s_a = s_0$), unlike the model of Enikeev and Kruglov[45] (Eq. [19]).

A comparison of measured and theoretical thickness strains for each model (Eqs. [19] and [21]) and for each material is presented in Figures 9(a) through (e). In most of the materials, the greatest variation between the experimentally determined strains and those predicted by Enikeev and Kruglov's[45] model occurs at the periphery of the dome, where the experimental data show little or no thickness reduction. In contrast, Ragab's model is in good agreement with experimental data at that location. Both models are fairly accurate at the apex, except in the case of Ti-6Al-4V/TiC$_p$.

The variation between the experimental data and the models could be caused by a temperature variation from the apex to the periphery, as discussed in the following. For the present experimental apparatus, there are several reasons why the dome periphery did not reach as high a temperature as the apex, leading to low thickness strains at the dome periphery. First, any pressurization gas leaks would probably occur at the dome periphery and would cause a decrease in temperature by convective cooling. Second, the large thermal mass of the pressurization vessel acts as a heat sink, drawing heat preferentially from the dome periphery; an analogous situation arises at the heads of a tensile specimen during radiant heating, leading to thermal gradients and lower strains in the gage near the heads.[56] Finally, the dome apex is closer to the heater and parallel to the incident radiation, while the periphery is more distant from, and at an inclined angle to, the heater, thus reducing the heat flux there. Since transformation superplasticity relies on the phase transformation to induce deformation, a partial transformation at the dome periphery due to lower temperature is expected to considerably reduce strains at this location. Also, a lower temperature would lead to a smaller creep contribution at the dome periphery.

V. CONCLUSIONS

The present study has investigated uniaxial and biaxial deformation by transformation superplasticity in unalloyed titanium (CP-Ti), a titanium alloy (Ti-6Al-4V), and three titanium matrix composites (Ti/10 vol. pct TiC$_p$, Ti-6Al-4V/10 vol. pct TiC$_p$, and Ti-6Al-4V/5 vol. pct TiB$_w$). Thermal-cycling experiments were performed while simultaneously subjecting specimens to an external stress, i.e., uniaxial tension of a cylindrical specimen or biaxial gas pressurization
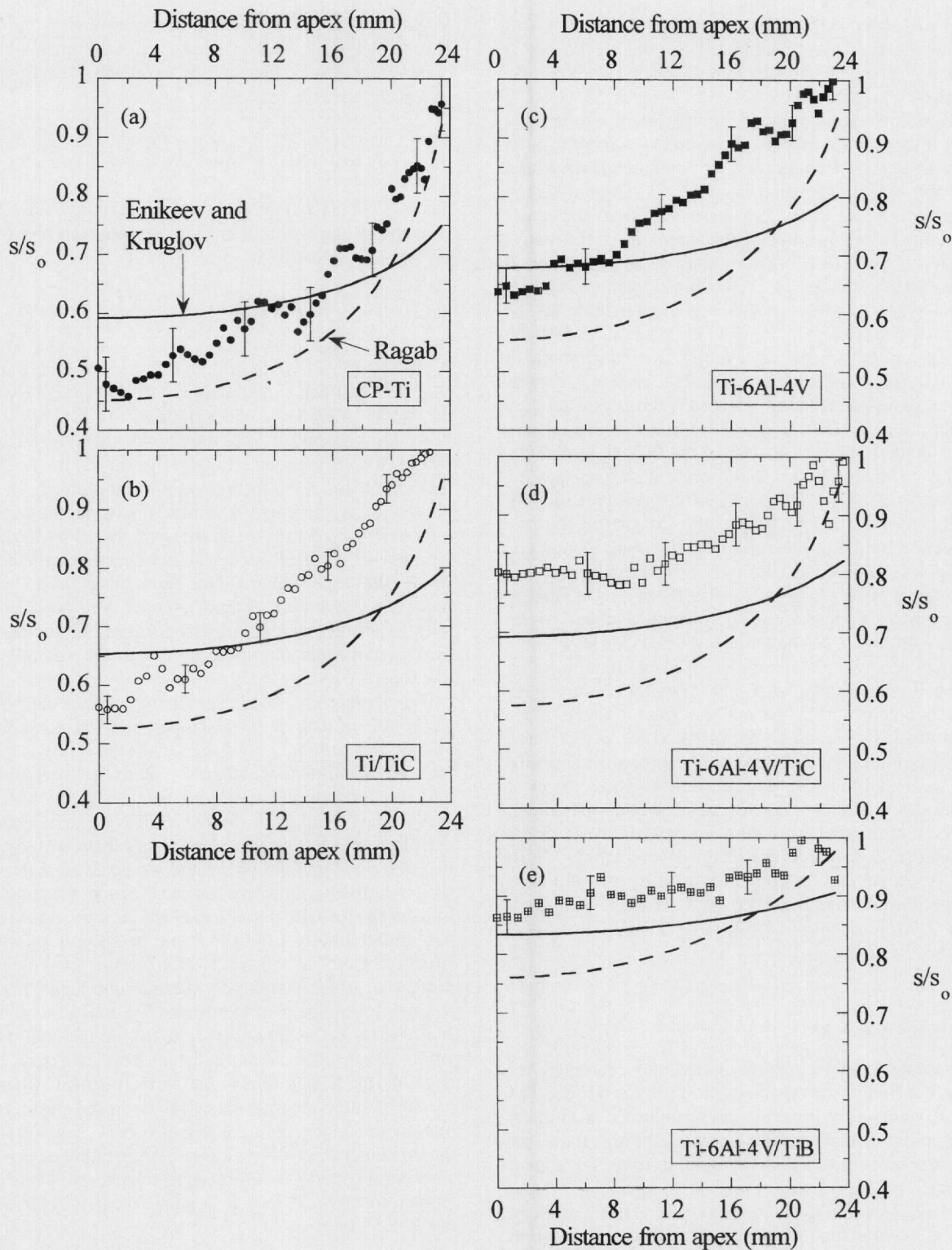
Fig. 9—(a) through (e) Comparison of experimental dome thickness data with the models of Enikeev and Kruglov (Eq. [19]) and Ragab (Eq. [21]).

of a sheet specimen. The major results are summarized as follows.

1. In uniaxial tension, thermal cycling through the Ti-α/β transformation range leads to a linear relationship between the strain increment accumulated after each cycle and the applied stress. Reinforcement additions

lower the cycling strain increments, primarily by increasing the transformation temperature range and causing partial phase transformation.

2. Biaxial deformation of titanium alloys and composites is enhanced by thermal cycling as compared to isothermal deformation. Local strains were determined by image analysis of deformed dome sections, and the maximum

engineering strain observed was 119 pct for CP-Ti. For three of the experimental materials (CP-Ti, Ti/TiC$_p$, and Ti-6Al-4V/TiB$_w$), these experiments constituted the first demonstration of biaxial transformation superplasticity.

3. Despite simplifying assumptions, analytical predictions based on the model of Enikeev and Kruglov[45] describes the dome growth kinetics and the measured thickness distributions of the deformed specimens with reasonable accuracy. The kinetic model also revealed the relative contributions of transformation superplasticity and creep during biaxial deformation and showed that deformation by isothermal creep alone would result in significantly longer times to attain the same degree of deformation as thermal cycling.

APPENDIX

One of the main assumptions of biaxial deformation modeling is that the dome can be described as part of a sphere at all times during deformation.[41–45] In order to test this assumption, circles were fitted to the experimental dome profiles (from the digitized coordinates of the upper surface, as described in Section II C3), with a radius equal to the radius of curvature of the dome, R (Fig. 6):

$$R = \frac{b^2 + h^2}{2h} \qquad [A1]$$

For each specimen, the measured dome shape was found to be very well described as part of a circle, as exemplified in Figure A1 for the deformed CP-Ti specimen. Equivalent or better agreement was found for all other domes.
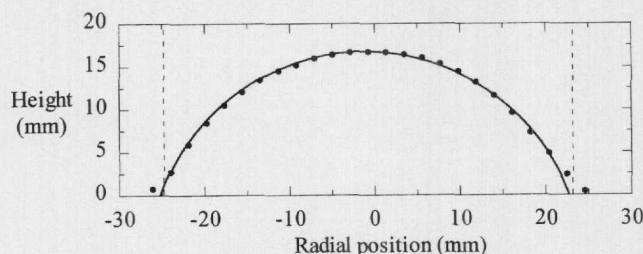

Fig. A1—Profile of CP-Ti dome, found by digital image processing on a cross section, fitted with a circle according to Eq. [A1]. Dashed lines indicate the diameter of the die opening through which the specimen could bulge.

REFERENCES

1. S. Lampman: in *ASM Handbook: Properties and Selection: Nonferrous Alloys and Special Purpose Materials*, ASM INTERNATIONAL, Metals Park, OH, 1990, p. 614.
2. T.G. Nieh, J. Wadsworth, and O.D. Sherby: *Superplasticity in Metals and Ceramics*, Cambridge University Press, Cambridge, United Kingdom, 1997.
3. G.W. Greenwood and R.H. Johnson: *Proc. R. Soc. London*, 1965, vol. 283, pp. 403-22.
4. C. Schuh and D.C. Dunand: *Acta Mater.*, 2001, vol. 49, pp. 199-210.
5. F.W. Clinard and O.D. Sherby: *Acta Metall.*, 1964, vol. 12, pp. 911-19.
6. A.G. Young, K.M. Gardiner, and W.B. Rotsey: *J. Nucl. Mater.*, 1960, vol. 2, p. 234.
7. D. Oelschlagel and V. Weiss: *Trans. Q. ASM*, 1966, vol. 59, pp. 143-54.
8. T.B. Massalski, S.K. Bhattacharyya, and J.H. Perepezko: *Metall. Trans. A*, 1978, vol. 9A, pp. 53-56.
9. M. de Jong and G.W. Rathenau: *Acta Metall.*, 1959, vol. 7, pp. 246-53.
10. M. de Jong and G.W. Rathenau: *Acta Metall.*, 1961, vol. 9, pp. 714-20.
11. R. Kot, G. Krause, and V. Weiss: in *The Science, Technology and Applications of Titanium*, R.I. Jaffe and N.E. Promisel, eds., Pergamon, Oxford, United Kingdom 1970, pp. 597-605.
12. C. Chaix and A. Lasalmonie: *Res Mechanica*, 1981, vol. 2, p. 241.
13. M. Lozinsky: *Acta Metall.*, 1961, vol. 9, p. 689.
14. K. Sato, T. Nishimura, and Y. Kimura: *Mater. Sci. Forum*, 1994, vols. 170-172, p. 207.
15. P. Zwigl and D.C. Dunand: *Metall. Mater. Trans. A*, 1998, vol. 29A, pp. 2571-82.
16. K. Nuttall and D.P. McCooeye: in *Mechanical Behavior of Materials*, The Society of Materials Science, Japan, 1974, pp. 129-40.
17. K. Nuttall: *Scripta Metall.*, 1976, vol. 10, pp. 835-40.
18. M. Zamora and J.P. Poirier: *Mech. Mater.*, 1983, vol. 2, pp. 193-202.
19. R.H. Johnson and G.W. Greenwood: *Nature*, 1962, vol. 195, pp. 138-39.
20. G.W. Greenwood and R.H. Johnson: *React. Sci. Technol.*, 1962, vol. 16, p. 473.
21. C. Schuh and D.C. Dunand: *Acta Mater.*, 1998, vol. 46, pp. 5663-75.
22. D.C. Dunand and C.M. Bedell: *Acta Mater.*, 1996, vol. 44, p. 1063.
23. C. Schuh and D.C. Dunand: *Scripta Mater.*, 1999, vol. 40, pp. 1305-12.
24. C. Schuh, W. Zimmer, and D.C. Dunand: in *Creep Behavior of Advanced Materials for the 21st Century*, R.S. Mishra, A.K. Mukherjee, and K.L. Murty, eds., TMS, Warrendale, PA, 1999, pp. 61-70.
25. C. Schuh and D.C. Dunand: *Int. J. Plasticity*, 2001, vol. 17, pp. 317-40.
26. C.A. Johnson, R.C. Bradt, and J.H. Hoke: *J. Am. Ceram. Soc.*, 1975, vol. 58, pp. 37-40.
27. D.C. Dunand and J.L. Grabowski: *J. Am. Ceram. Soc.*, 2000, vol. 83, pp. 2521-28.
28. O.A. Ruano, J. Wadsworth, and O.D. Sherby: *Metall. Trans. A*, 1982, vol. 13A, pp. 355-61.
29. C. Schuh, P. Noël, and D.C. Dunand: *Acta Mater.*, 2000, vol. 48, pp. 1639-53.
30. D.C. Dunand and J. Teisen: in *Porous and Cellular Materials Structural Applications*, D.S. Schwartz, D.S. Shih, H.N.G. Wadley, and A.G. Evans, eds. MRS, Pittsburgh, 1998, pp. 231-36.
31. N.G. Davis, J. Teisen, C. Schuh, and D.C. Dunand: *J. Mater. Res.*, 2001, vol. 16, pp. 1508-19.
32. D.C. Dunand and S. Myojin: *Mater. Sci. Eng.*, 1997, vol. A230, pp. 25-32.
33. S. Abkowitz and P. Weihrauch: *Adv. Mater. Processes*, 1989, vol. 7, pp. 31-34.
34. S. Abkowitz, P.F. Weihrauch, and S.M. Abkowitz: *Industrial Heating*, 1993, vol. 12, pp. 32-36.
35. M.E. Hyman, C. McCullough, J.J. Valenci, C.G. Levi, and R. Mehrabian: *Metall. Trans. A*, 1989, vol. 20A, pp. 1847-59.
36. T. Saito: *Advanced Performance Materials*, 1995, vol. 2, pp. 121-44.
37. K. Funami, M. Kobayashi, S. Suzuki, and C. Ouchi: *Mater. Sci. Forum*, 1997, vols. 243–245, pp. 515-20.
38. M. Frary: Master's Thesis, Northwestern University, Evanston, IL, 2001.
39. W. Szkliniarz and G. Smolka: *J. Mater. Processing Technol.*, 1995, vol. 53, pp. 413-22.
40. C. Schuh and D.C. Dunand: *Mater. Sci. Forum*, 2001, vols. 357–359, pp. 177-82.
41. F. Jovane: *Int. J. Mech. Sci.*, 1968, vol. 10, pp. 403-27.
42. A.R. Ragab: *Met. Technol.*, 1983, vol. 10, pp. 340-48.
43. S. Yu-Quan and Z. Jun: *Mater. Sci. Eng.*, 1986, vol. 84, pp. 111-25.
44. Z.X. Guo and N. Ridley: *Mater. Sci. Eng.*, 1989, vol. A114, pp. 97-104.
45. F.U. Enikeev and A.A. Kruglov: *Int. J. Mech. Sci.*, 1995, vol. 37, pp. 473-83.

46. C.F. Yang, L.H. Chiu, and S.C. Lee: *Scripta Mater.*, 1996, vol. 34, pp. 1555-60.
47. *Binary Alloy Phase Diagrams*, T.B. Massalski, ed., ASM INTERNATIONAL, Metals, Park, OH, 1990.
48. A.K. Ghosh and C.H. Hamilton: *Metall. Trans. A*, 1982. vol. 13A, pp. 733-43.
49. A. Dutta and A.K. Mukherjee: *Mater. Sci. Eng.*, 1992, vol. A157, pp. 9-13.
50. T.H. Courtney: *Mechanical Behavior of Materials.* McGraw-Hill, Inc., New York, NY, 1990.
51. I. Finnie and W.R. Heller: *Creep of Engineering Materials.* McGraw-Hill Book Company, Inc., New York, NY, 1959.
52. H.J. Frost and M.F. Ashby: *Deformation Mechanism Maps.* Pergamon Press, Oxford, United Kingdom, 1982.
53. C. Schuh and D.C. Dunand: Northwestern University, Evanston, IL, unpublished research, 2000.
54. S. Ranganath and R.S. Mishra: *Acta Mater.*, 1996, vol. 44, pp. 927-35.
55. S.J. Zhu, Y.X. Lu, Z.G. Wang, and J. Bi: *Mater. Lett.*, 1992, vol. 13, pp. 199-203.
56. C. Schuh and D.C. Dunand: *J. Mater. Res.*, 2001, vol. 16, pp. 865-75.